Diyala Journal of Engineering Sciences

Journal homepage: https://djes.info/index.php/djes

ISSN: 1999-8716 (Print); 2616-6909 (Online)

Effect of Mass Flow Rate in a Shell and Tube Heat Exchanger of Different Inner Tube Geometries during Solidification of Phase Change Material

Abdulrazzaq M. Saleh Aljumaily[1*], Akeel A. Mohammed[2] and Sattar J. Aljabair[3]

[1]Department of Mechanical Engineering, College of Engineering- Alshirqat, Tikrit University, Salah-Al-din, Iraq
[2]Department of Mechanical Engineering, College of Engineering, Al-Nahrain University, Baghdad, Iraq
[3] Department of Mechanical Engineering, University of Technology, Baghdad, Iraq

ARTICLE INFO

Article history:
Received June 9, 2024
Revised August 16, 2024,
Accepted August 19, 2024,
Available online December 1, 2024

Keywords:
Energy storage
Elliptical with minor axis bending
Different inner tube
Phase change material
Solidification

ABSTRACT

The current work consists of a theoretical and experimental investigation of the impact of mass flow rate on the solidification process of phase change materials (PCM) for various inner tube geometries of heat exchangers. The heat exchanger consists of an outer shell filled with paraffin wax as a PCM. Simultaneously, three tested inner tube shapes with the same cross-sectional area are circular, elliptical with minor axis bending, and elliptical with major axis bending. Water was used as the heat transfer fluid (HTF) at two and four L/min flow rates inside the inner tube. A three-dimensional ANSYS simulation was constructed to examine the thermal behaviour of heat exchangers incorporating PCM. The findings demonstrated that when the mass flow rate of HTF decreased, so the solidification time increased. Furthermore, compared to other tube forms, circular tubes offer longer-lasting heat absorption from phase shift materials through the heat transfer fluid. Also, the results show that the heat transfer process between PCM and HTF is controlled by natural convection. solidification begins near the inner tube and then moves towards the casing (horizontal axis at 0°, then inclined axis at 45°, followed by the vertical axis at 90°). Moreover, it was observed that the maximum theoretical and experimental thermal efficiencies recorded were (67.7%, 71.6%,) for the circular inner tube followed by (49.2%, 53.2%) for the elliptical inner tube with minor axis bending and (44.6%, 48.1%) for the elliptical inner tube with major axis bending at a water volumetric flow rate of 2 L/min, respectively.

1. Introduction

Due to the escalating demand for energy and the exhaustion of traditional energy sources, a global energy crisis has emerged. Additionally, these resources possess limited quantities, and there is a rising trend in fuel costs and environmental apprehensions [1]. Thermal energy storage systems (TESS) must be developed in order to handle the problems that come up when producing and using energy. Among these storage systems, the most suitable option for this usage is the latent heat storage systems (LHSS) based on phase change materials (PCM). Several computational and experimental investigations have been carried out to improve and optimize the thermal behavior of LHSS devices [2-4]. PCM such paraffin wax [5] and erythritol [6] in vertical and horizontal heat exchangers for latent heat thermal storage units [7, 11] is also employed. Mahdi et al. [12] conducted a comparison between two scenarios: inserting the PCM in the inner tube and placing it in the annulus. It was

* Corresponding author.
E-mail address: Abdularrazq9220@gmail.com
DOI: 10.24237/djes.2024.17408

discovered that the process of solidification takes a lengthier amount of time when the substance is placed in the inner tube compared to when it is placed in the annulus. Sadeghi et al. [13] recommended increasing the number of PCM layers in order to effectively absorb a significant amount of thermal heat in its latent form. Liu et al. [14] and Elmeriah et al. [15] found that the discharging operation of stearic acid is little influenced by the Reynolds number of HTF (water). Avci, et al. [16] and Agarwal et al. [17] also found that the charging operation of PCM occurs radially upwards because of buoyancy force. Furthermore, the upper zone arrives at the melting point before the lower zone. Seddegh et al. [18] concluded the natural convection plays a significant role in the heat transfer process during the solidification phase. The observed phenomenon was attributed to the influence of buoyant forces, as documented by Jesumathy et al. [19]. Hosseini et al. [20], was found that as the temperature of HTF increases, the rate at which the melt front progresses from the pipe to the shell increases, leading to a reduced duration of the melting process. In contrast, the discharging time increased due to the used of eccentric geometric shapes for the inner tube [21] and it reducing with increased the number of tubes inside the shell Esapour, et al. [22].

A conduction-convection model is created to examine the impact of natural convection within PCM during the melting and solidification stages of a cascade Latent Heat Thermal Energy Storage System (LHSSS). This model is then compared to a pure conduction model. The phase change processes in both mixed model and pure conduction models are simulated using the effective heat capacity approach. The simulation findings showed that at higher intake velocity of HTF, the heat transfer processes inside PCM are mostly governed by conduction. The findings also indicated that the intake temperature of HTF significantly influences the reduction in the time required for charging and discharging [23].

Aljumaily et al. [24] presented theoretical and practical investigations to improve thermal storage system thermal efficiency by changing inner tube geometry. Pentagonal, hexagonal, square, rectangular, and circular with the same exterior surface area were chosen. The shell contains phase transition ingredient paraffin wax, while water, a Heat Transfer Fluid, flows through the inner tube at two liters per minute. All chosen geometric shapes were simulated in 3D using ANSYS Fluent 2020 R2 [25]. Using the HTF, the circular tube absorbed heat from the PCM better than the other types. Furthermore, increased in the average Nusselt number with increased the number of tubes inside the shell [26]. According to Shen, et al. [27], the positioning of the heat transfer fluid tubes can impact the thermal characteristics of a multi-tube storage unit. The radius of the pipes had a significant impact on the discharging/charging time as noted Kibria, et al., [28]. While, the shell/reduce model had the lower period in strong convection, followed by the shell/tube model and then the nozzle/shell model Korawan et al. [29]. Seddegh et al. [30] used numerical simulation to confirm these findings. The influence of altering the angle of inclination on a heat exchanger filled with PCM such as (paraffin wax in Kousha et al. [31], steric acid in Mehta et al. [32]), paraffin wax-fins inner tube Siyabi et al. [33], and copper nanoparticles and steel/nickel alloys as porous media Jourabian et al. [34] were examined. The results showed a decrease in the PCM temperature with an increase in the tilt angle of the thermal storage unit from 00 to 900. Ajarostaghi et al [35] conducted a numerical study on the impact of different inner tube geometries. The results indicate a substantial enhancement in heat transmission for a semicircular heat exchanger as compared to the inner tube of a conventional tube-in-tube heat exchanger. The convection connection of the copper plate between the moving fluids can account for this phenomenon. The expanded fins on either side of the heat exchanger are virtually visible. Additionally, Da Veiga and Meyer [36] found that using a semicircular heat exchanger leads to significant improvements in heat transfer compared to a traditional tube-in-tube heat exchanger. Albaldawi et al. [37] found that the addition of copper Lessing rings with PCM reduces the time of melting operation in the LHSS unit. In addition, Longeon et al. [38]

employed graphite foam to enhance the thermal conductivity of PCM in heat exchangers with finned inner. While the insertion of metallic foam and adding the number of tubes leads to an enhancement rate of discharging and charging, as noted by Esapour et al. [39]. In addition, the increase in the Biot number led to a decrease in the efficiency of the heatsink, as mentioned by Ghalambaz, and Zhang et al. [40]. As demonstrated by Wang et al. [41] and Begum et al. [42], the solidification and melting operation of hexagon/tube and shell/tube systems is significantly influenced by the mass flow rate and inlet temperature of HTF. Thus, Akgu¨n et al. [43] suggested utilizing a reduced mass flow rate of HTF. Furthermore, it has been observed by Jian-you [44] that the charging time decreases as the HTF's inlet temperature rises [45-47]. A computational technique known as "alternative iteration between temperature and thermal resistance" was created by Kibria et al. [48] to investigate the heat transfer in these systems between the PCM and the HTF. While, Hamza and Aljabair [49] evaluation of thermal performance factor by hybrid Nano fluid and twisted tape inserts in heat exchanger.

This study aims to investigate the effect of mass flow rate on different inner tube geometries both theoretically and practically. The shapes consist of a circular tube, an elliptical inner tube with a bend along the major axis and an elliptical inner tube with a bend along the minor axis. In addition, to examining the thermal characteristics of the LHSS unit during solidification process. To ensure laminar flow, a water flow rate of 2 and 4 L/min was selected.

2. System description

Figure 1. and 2 show the schematic diagrams of LHSSs with the PCM which consists an aluminum shell with the following dimensions (1.5 mm thick, 1-meter-long, and 160 mm in diameter). The shell was partitioned into three distinct areas, namely A, B, and C, each region containing holes distributed at different angles (90 degrees, 45 degrees, and 0 degrees) to fix the (36) thermocouples in different locations. Three concentric shapes were used inside the shell. The first shape is a circular tube with the following dimensions (1.5 mm thick, 1500 mm long, and 54 mm in diameter). The second shape is an elliptical inner tube with a major axis bending. It has dimensions of 60 mm for the main diameter, 47.5 mm for the secondary diameter, and a length of 1,5 m. The third shape consists of an elliptical inner tube that is bent along its minor axis, while keeping the same dimensions as the second variant. All the tested shapes are made of copper and the working fluid inside the tubes is water (see Figure 3). While, the paraffin wax from Al-Daura Refinery / Iraq with the thermal physical properties in Table 1. The shell is surrounded by four ring heaters with the following specifications (diameter 160 mm and 2160 watts) for melting paraffin wax. The shell was insulated with asbestos tape with the following specifications (0.05 m thick and 0.37 W/m thermal conductivity rate). As well as KYMCO pipes with the following specifications (with a thermal conductivity ratio of 0.037 W / m, a length of 1 meter, and a diameter of 178 mm).

Table 1: Utilized materials' thermo-physical properties

Materials Properties	PCM	Water	Aluminum	Copper	Insulation
Melting temperature [K]	334	-	-	-	-
Density in solid state [kg/m^3]	894.56	-	2719	8978	-
Density in liquid state [kg/m^3]	783.42	998.2	-	-	-
Specific heat in solid state [J/kg K]	1659	-	871	381	-
Specific heat in liquid state [J/kg K]	2460	4182	-	-	-
Latent heat of fusion [J / kg]	235512.5	-	-	-	-
Thermal conductivity in solid state [W / m K]	0.259	-	202.4	387.6	0.043
Thermal conductivity in liquid state [W / m K]	0.158	0.6	-	-	-
Dynamic viscosity [kg/m.s]	0.01405	0.001003	-	-	-
Solidus temperature [K]	318.5	-	-	-	-
Liquidous temperature [K]	339	-	-	-	-
Thermal expansion coefficient [1/K]	0.000307	-	-	-	-

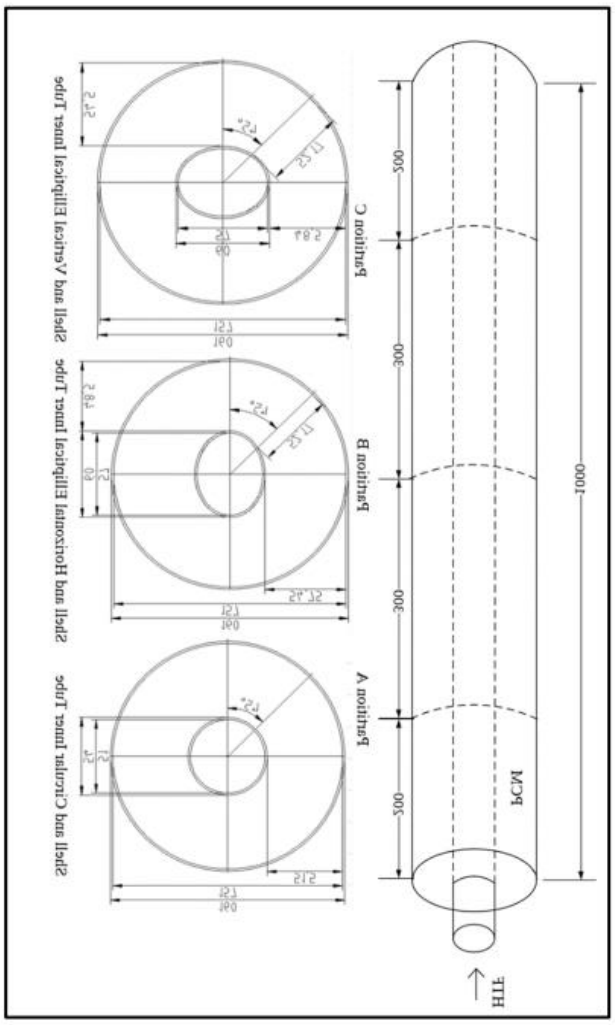

Figure 1. Shell and tube geomtries considered for the study

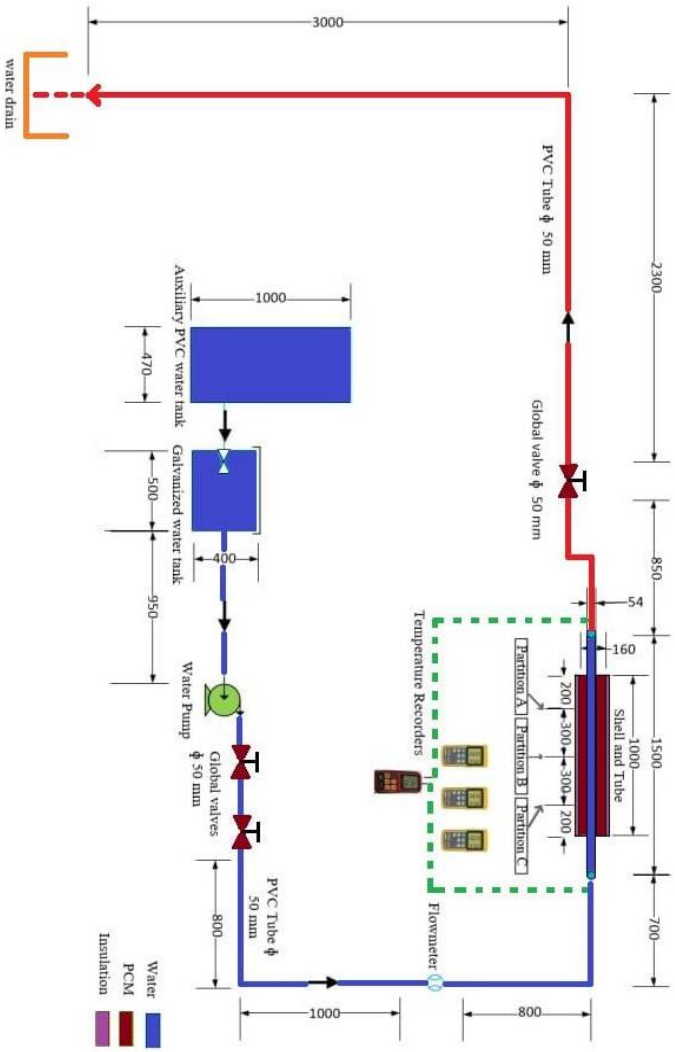

Figure 2. An illustration of the experimental system, with all dimensions given in millimeters

Figure 3. Photo of the shell and tube heat exchanger used in the study

The equation for the instantaneous energy transferred can be expressed as follows: during the solidification and melting process, from the PCM to the heat transfer fluid [12,50,51]:

$$q_{dis} = \dot{m}.C_P.(T_{f,out} - T_{f,in}) \quad (1)$$

$$Q_{dis} = \sum q_{dis}\Delta t \quad (2)$$

The variables C_P and m represent specific heat and the mass flow rate of HTF respectively. $T_{f,in}$ and $T_{f,out}$ refer to the temperatures of the entering and outlet water, while transient state operation, the equation for energy accumulation while charging and discharging can be expressed as follows [12,51]:

$$Q_{h.e,,diS} = M_{h.e}.C_{p,H.E}.(T_{ini} - T_{end}) \quad (3)$$

Where T_{end} and T_{ini} are end, initial of paraffin wax temperature, $C_{p,H.E}$, $M_{H.E}$ are specific heat and mass of the empty heat exchanger. The cumulative energies exchangeable with paraffin wax can be expressed as follow [12.51]:

$$Q_{,dis,PCM} = Q_{dis} - Q_{dis,h.e,} \quad (4)$$

The LHSS's theoretical efficiency is expressed as follows [12,51]:

$$\eta_{THEO} = \frac{Q_{dis,PCM}}{Q_{,dis,max}} \quad (5)$$

For the solidification and melting process, the theoretical maximum energy, or total energy received or delivered by the PCM, can be expressed as follows [12,51].

$$Q_{,dis,max} = M_{pcm}[C_{P\ pcm}.(F.L).(T_{liquidus} - T_{solidus}) + C_{P\ pcm}.(T_{ini} - T_{liquidus})] \quad (6)$$

Where is the difference between the liquidus temperature ($T_{liquidus}$) and the solidus temperature ($T_{solidus}$) of PCM, the M_{pcm}, $C_{P\ pcm}$ are the mass and specific heat of paraffin wax, (L) the latent heat of fusion and (F) liquid fraction.

3. Numerical simulation

The ANSYS-Fluent 2020 R 2 software was utilized to model the solidification process of PCM for varied inner tube geometries under varying flow rates. In order to maintain stability and equilibrium at the boundary between the liquid and solid phases, a technique known as the enthalpy method was employed during the process of discharging the PCM [12,14]. The analysis takes into account the following assumptions: The unsteady state condition in three dimensions: (II) The flow of the heat transfer fluid is described by Newtonian fluid behavior, with laminar flow and being incompressible. (III) The phase change material is uniform throughout and has the same properties in all directions. (V) The water's input temperature (HTF) remains constant at 299 K; (VI) The influence of viscous dissipation is deemed negligible. (VII) The shell's outer surface is completely insulated, preventing any heat from being lost to the surrounding environment. Heat transfer occurs exclusively between HTF and PCM.

The equation for total volumetric enthalpy and temperature can be represented by the following expression [12] [51]:

$$\frac{\partial \rho H}{\partial t} + \nabla.(\rho V H) = \nabla.(K\nabla T) + C \quad (7)$$

The symbol H indicates the total volumetric enthalpy, which includes both latent and sensible heat. The symbol k represents thermal conductivity, ρ represents the density of the paraffin wax, *V* represents the velocity and the source term is C [51].

$$H = FL + H \quad (8)$$

$$H = \int_{TREF}^{T} C_P\, dT + H_{REF} \quad (9)$$

In the mushy zone, where the liquid percentage (F) ranges from 0 to 1,$T_{REF,}$ temperature reference 299 K, H_{REF} enthalpy of reference, and C_p specific heat, temperature.

$$F = \begin{cases} 0 & T < T_S \\ \frac{T-T_S}{T_L-T_S} & T_S \le T \le T_L \\ 1 & T > T_L \end{cases} \quad (10)$$

The energy equation after Substantial Eq. 2 and 4 into Eq. 1 being as followed [51].

$$\frac{\partial \rho H}{\partial t} + \nabla.(\rho VZ) = \frac{\partial \rho FL}{\partial t} - \nabla.(\rho VFL) - \nabla(K\nabla T) + C \quad (11)$$

The momentum equation can be expressed as [51]:

$$\frac{\partial \rho v}{\partial t} + \nabla(\rho vv) = -\nabla P + \nabla(\mu \nabla V) + \rho g + \frac{(1-F)^2}{F^3+\varepsilon} V A_{mush} \quad (12)$$

Where L is the latent heat fusion, $A_{mush} = 10^5$ is the soft region constant that functions as a velocity-damping factor during PCM discharging, and $\varepsilon = 0.001$ is a tiny value that is not divisible by zero.

To solve the problem of the little density difference, their method is called The Boussinesq approximation is a mathematical simplification used in fluid dynamics to model the behaviour of a fluid with small density variations. This method is based on the assumption that the density of the fluid remains constant, and it does not take into account the effects of body force in the momentum equation.

Then the momentum equation can be expressed as [51].:

$$\frac{\partial \rho_0 v}{\partial t} + \nabla.(\rho_0 vv) = (\rho - \rho_0)g + \frac{(1-F)^2}{F^3+\varepsilon} vA_{mush} - \nabla P + \nabla.(\mu \nabla v) \quad (13)$$

$$\beta \rho_0 (T - T_0) = (\rho - \rho_0) g \quad (14)$$

The continuity can be calculated form [51]:

$$\nabla.(\rho v) + \frac{\partial \rho}{\partial t} = 0 \quad (15)$$

3.1 Numerical Setup

A Computational Fluid Dynamics is a method of studying and solving problems in fluid mechanics using information combination and numerical analysis. The inner pipe is built with three different geometries: an elliptical inner tube with bending along the major axis, an elliptical inner tube with bending along the minor axis, and a circular pipe. In order to enhance the accuracy of numerical simulation outcomes and reduce the margin of error. The mesh independence test was conducted by choosing different numbers of sample mesh elements (5) and determining the mass percentage that ensures the calculations do not diverge. According to the results, the mesh element sizes for the various shapes—a circular tube, a shell, a shell with an elliptical inner tube bending major axis, and an elliptical inner tube bending minor axis—were, in that order, 1452238, 1103634, and 1099818 (see Figure 4). Additionally, the transitory formulation employs a first-order implicit method, Density, pressure, body forces, liquid fraction, momentum update, and energy have the following respective relaxation factors: 1, 0.3, 1, 0.9, 0.7, and 1. A second-order upwind approach was used to estimate the momentum and energy equations, while a second-order method was used to estimate the pressure energy equation. Furthermore, the pressure and velocity coupling was chosen using the SIMPLE technique, to resolve equations and simulate the process of solidification and distribution of temperature for various geometric forms. Figure 5 and Table 2 display the parameters used to simulate the specified chosen.

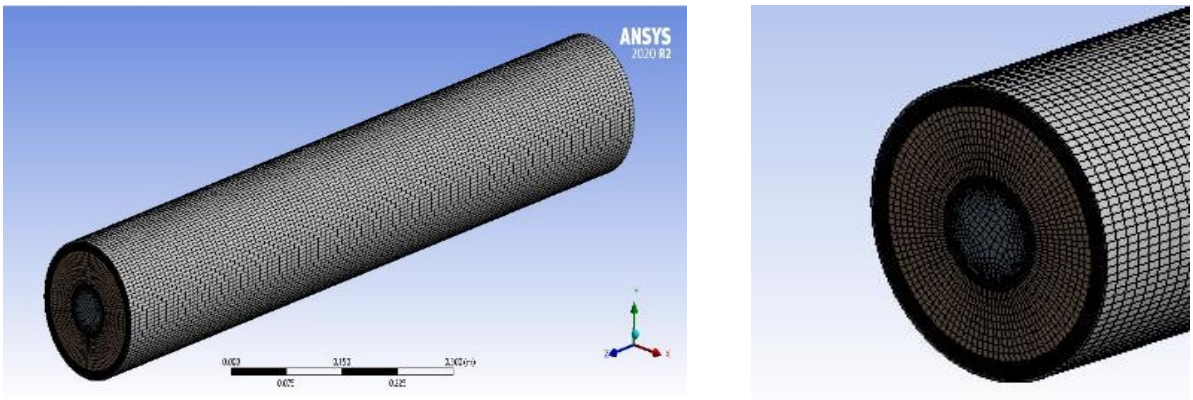

A

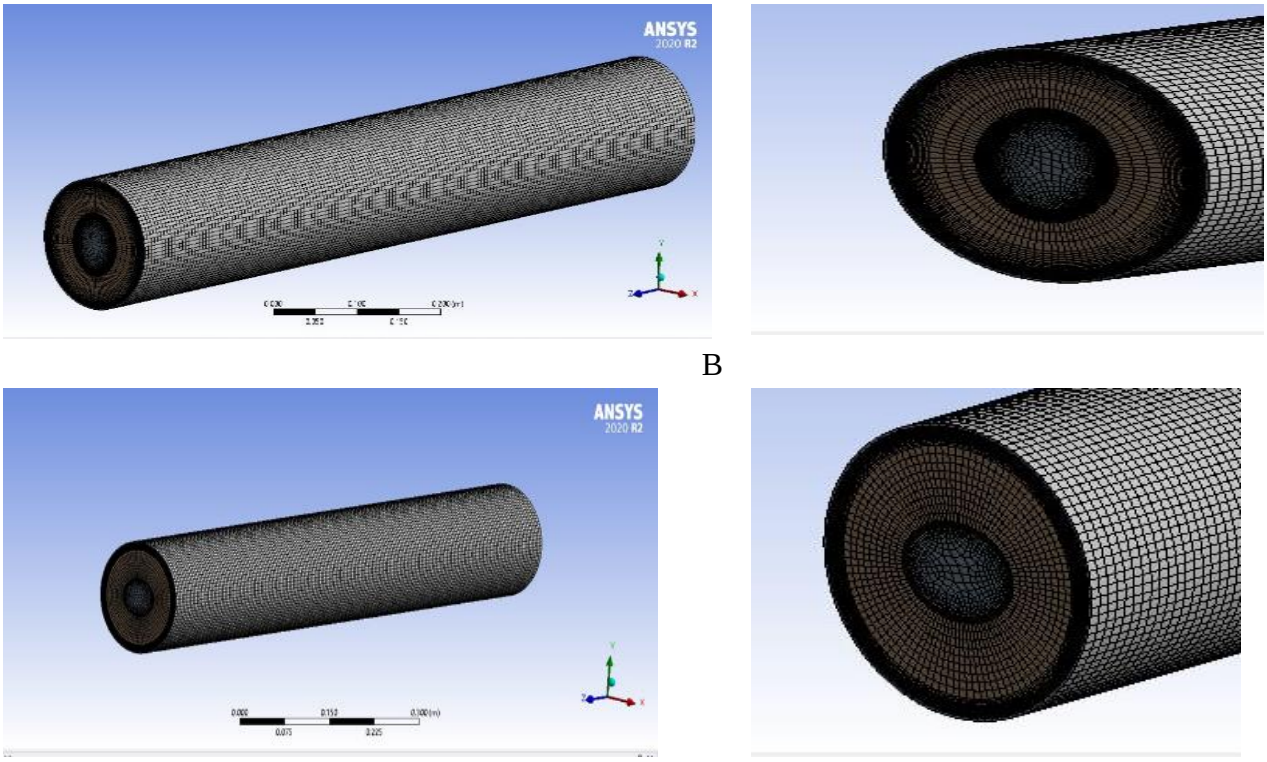

Figure 4. Mesh Generation of (A) Circular Tube-Shell, (B) Elliptical Inner Tube with Major-Shell, and (C) Minor Axis Bending-Shell

The current work involves the development of 3-D models to simulate different states. This process consists of four parts, which are as follows:

During the melting process, the heat flux measured 4300 W/m^2. The solidification process occurs at a temperature of 299 K. Also, all walls, save for the one between the HTF and PCM, were assumed to be insulated. Furthermore, this specific condition has been selected to enhance the exchange of thermal energy between the PCM and HTF. Moreover, the material and thickness of each wall were determined. The gauge pressure at the exit was set to zero Pascal's, and the boundary condition was defined as the outflow boundary for the heat transfer fluid. In addition, the chosen boundary condition type at the inlet is speed entry (HTF). The time step size is 0.05 seconds. The iteration limit was set to 10, the initial temperature was set to 345 K and the time step was 500,000.

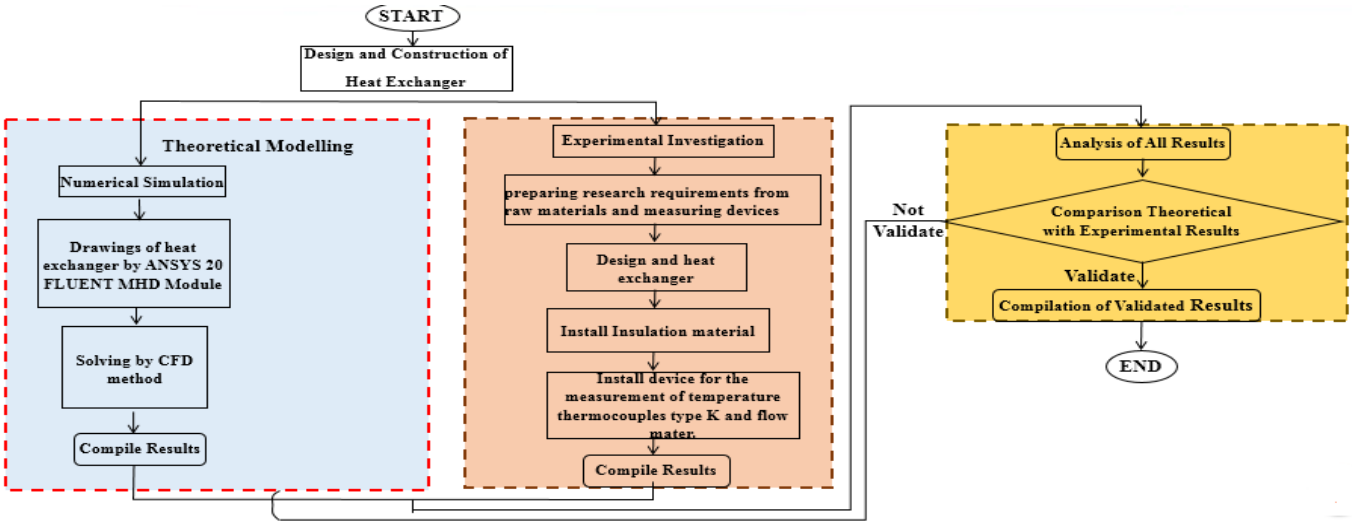

Figure 5. Flow chart of experiment and simulation

Table 2: Characteristics of every geometric shape put to the test

Geometrical Shapes Models	Volume Flow Rate of HTF (L / min)	Velocity m / sec	Reynolds Number
Shell /Circular Tube	2	0.01631	952.363
Shell /elliptical inner tube with major axis bending	2	0.0172	978.024
Shell /elliptical inner tube with minor axis bending	2	0.0172	978.024
Total Number of Tests	3		

In order to achieve robust practical results, it is necessary to calculate the reliability of the outputs. There are other investigators who have introduced various ways for uncertainty analysis. The technique involves considering the uncertainties associated with each of these characteristics in order to accurately calculate the overall investigative error. To calculate the investigative error, a parameter such as T, produced from an applied examination, can be linked to a series of independent parameters (S_1, S_2, S_3, ..., S_n), and so on **[**52**].**

$$T = T(S_1, S_2, S_3, ..., S_n) \quad (16)$$

And, the subsequent formula states the relation between the proportions of certain discrepancies in the parameters.

$$\partial N = \frac{\partial T}{\partial S_1}\partial S_1 + \frac{\partial T}{\partial S_2}\partial S_2 + \cdots + \frac{\partial T}{\partial S_n}\partial S_n \quad (17)$$

Also, results (N_T) uncertainty is stated by:

$$N_T = \left[\left(\frac{\partial T}{\partial S_1}N_1\right)^2 + \left(\frac{\partial T}{\partial S_2}N_2\right)^2 + \left(\frac{\partial T}{\partial S_n}N_n\right)^2\right]^{\frac{1}{2}} . \quad (18)$$

Dividing equation (12) by equation (10) gives

$$\frac{N_T}{T} = \left[\left(\frac{\partial T}{\partial S_1}\frac{N_1}{T}\right)^2 + \left(\frac{\partial T}{\partial S_2}\frac{N_2}{T}\right)^2 + \left(\frac{\partial T}{\partial S_n}\frac{N_S}{T}\right)^2\right]^{\frac{1}{2}} . \quad (19)$$

And, the created errors via the measuring devices of temperature as well as rate of flow rate being (±0.75%) and (±4%) for the temperature and rate of mass flow, correspondingly. In addition, the quantity of error investigated for the rate of heat transfer formula relies upon numerous variables.

$$\dot{Q} = F(\Delta T, \dot{m}) \quad (20)$$

$$\frac{\partial Q}{\partial \dot{m}} = C_P \Delta T \quad (21)$$

$$\frac{\partial Q}{\partial \Delta T} = C_P \dot{m} \quad (22)$$

And, heat transfer (N_Q) uncertainty is stated as:

$$\frac{N_Q}{Q} = \left[\left(\frac{\partial Q}{\partial \dot{m}}\frac{N_{\dot{m}}}{Q}\right)^2 + \left(\frac{\partial Q}{\partial\, \Delta T}\frac{N_{\Delta T}}{Q}\right)^2\right]^{\frac{1}{2}} \quad (23)$$

Where:

$$N_{\dot{m}} = error_{\dot{m}}\dot{m} \quad (24)$$

$$N_{\Delta T} = error_{\Delta T}\Delta T \quad (25)$$

Substituting the whole terms values into equation (23) gives

$$\frac{N_Q}{Q} = 6\%$$

4. Results and discussions

A study was conducted to investigate the effects mass flow rate of different geometrical shapes of inner tubes (elliptical inner tube with minor axis bending, circular tube, and elliptical inner tube with major axis bending) on the discharge performance of an LHSS unit. Specifically, this involves a comparison between the experimental and simulation methodologies. There was a total of 6 tests conducted.

4.1 Validation case study

A comparison was conducted between the findings of this study, specifically the solidification process of PCM through a circular tube, and the results of previously published research [51]. In their work, Seddegh et al. [51] conducted a numerical analysis of energy storage utilizing a horizontal shell-and-circular inner tube configuration, employing Paraffin Wax (RT 50) with a melting temperature range of 318-324 K. The experiment was conducted with a water flow rate of 2.5 l/min. The shell was constructed using iron, with an interior diameter measuring 85 mm and a thickness of 2.5 mm. The inner tube, composed of copper, was positioned at the center with a diameter of 22 mm. This study investigated a heat exchanger consisting of Paraffin wax, which has a melting temperature of 345 K, and an aluminum shell with an inner diameter of 160 mm and a thickness of 1.5 mm. The inner tube, composed of copper, was positioned at the center with a

diameter of 54 mm. Both investigations utilized water as the heat transfer fluid (HTF) that cycled through the inner tube. The findings demonstrated a strong alignment between the current and prior results, as depicted in Figure 6 and Table 3. Furthermore, the results demonstrated a strong correlation between the experimental investigations of thermal efficiency and numerical simulation, as depicted in Figure 6.

Table 3: Comparison results for validation case study

Mass fraction	Time (min) for Present results	Time (min) for Results of [51]
0.99	1	1
0.5	112	120
0	397	450

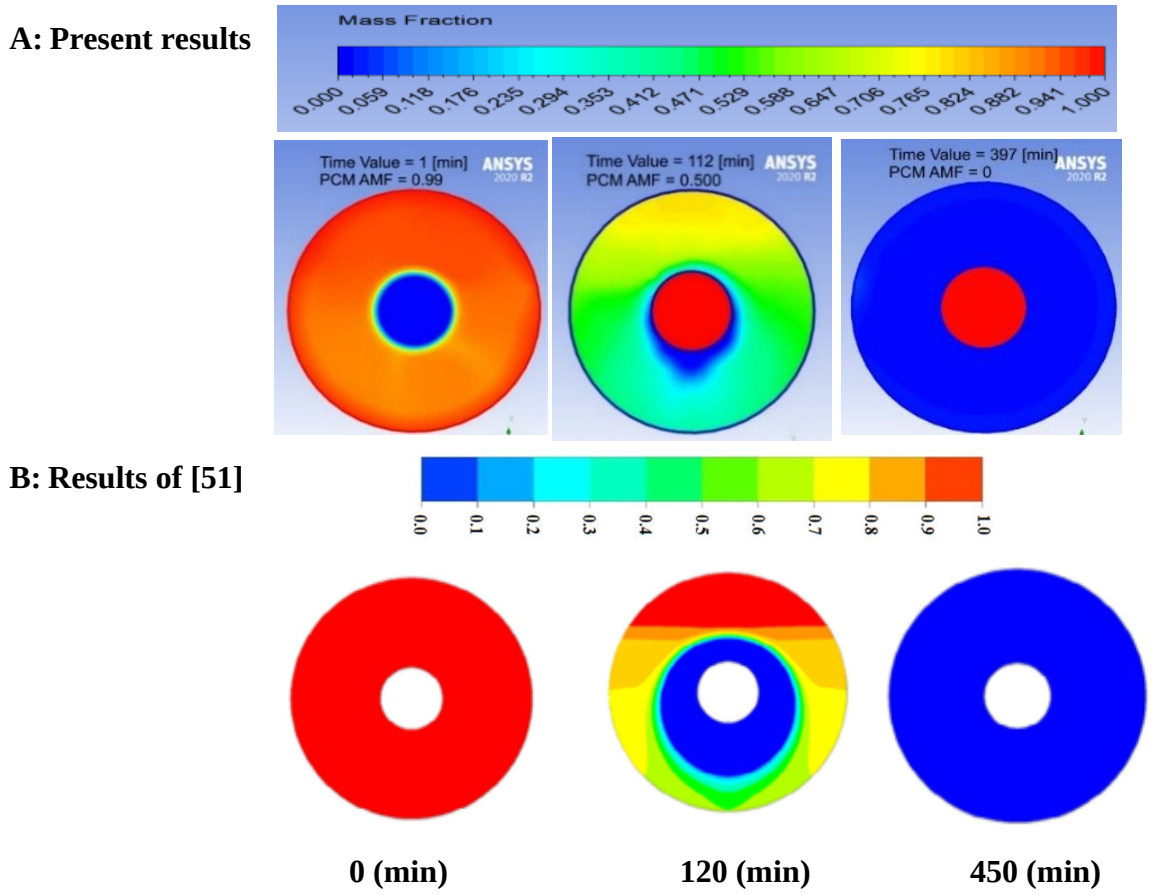

Figure 6. Numerical validation for the contours of the fraction of liquid during discharging in a horizontal regime

4.2 Present case study

When the melting process is completed and the PCM temperature reaches 345 K, cold water is pumped in to start the solidification process. After that, the readings are recorded after every two minutes. For all tested geometries, Figure. 7 shows the results of the average mass fraction (AMF) values at (1, 0.5, and 0) during the solidification process. The results show that the heat transfer process between PCM and HTF is controlled by natural convection. solidification begins near the inner tube and then moves towards the casing (horizontal axis at 0°, then inclined axis at 45°, followed by the vertical axis at 90°). Then the conduction dominates the heat transfer because of the PCM's increased solidification layer thickness and decreased thermal conductivity in the vicinity of the wall of the HTF tube, thus the solidification time is increased. For a concentric elliptical inner tube with major axis bending/shell at 2 L/min, Similar trend is shown to was previously described. However, the temperature

distribution and liquid mass fraction contours over radial distance show that discharging is faster than in the circular inner tube scenario. In addition, the liquid portion of paraffin wax declines after discharging (0.98 at 1 min, 0.74 at 22 min, 0.50 at 83 min, 0.25 at 306 min, and 386 min). while a concentric elliptical inner tube with a minor axis bending and 2 L/min HTF volumetric flow, the liquid fraction and temperature show behave similarly as mentioned above. These figures demonstrate the discharge time reduction with radial distance compared to other geometric shapes. For all test geometry at 4 L/min, the results demonstrate the same performance as previously described for the same mass flow rate, see Figure 8. Although, the contour of the liquid mass fractions indicate that the discharging time is shorter in comparison to the same case at a mass flow rate of 2 L/min, see Figure 9.

Figure 10 shows the numerical temperature distribution for all tests of geometry shapes at 2, 4 L/min. The temperature of the PCM gradually decreases in all parts until the fluid percentage hits 0.25, at which point solidification becomes evident first on the horizontal axis (0°) then the inclined axis (45°), and finally the vertical axis (90°). The outcomes showed that the other two models had the same pattern. The solidification times did, however, varied noticeably, with the (shell / elliptical inner tube with slight axis bending) exhibiting a faster solidification time compared to the (shell / elliptical inner tube with major axis bending) and the (shell / circular tube). Furthermore, it can be observed that the temperatures at section A exhibit a greater decrease compared to those at section B and section C (see Figure 11). This discrepancy may be attributed to the significant heat transfer occurring between HTF and PCM in the first segment of the experimental heat exchanger, as depicted in Figure 12.

When water at a temperature of 299 Kelvin is forced through a pipe inside a container, the material inside the container that undergoes a change in state starts to become solid. The transmission of heat from PCM to HTF in the inner tube leads to a gradual decrease in the liquid portion of PCM. The heat transfer initially takes place by convection and subsequently through conduction when the paraffin undergoes a phase transition from liquid to solid. As the PCM undergoes solidification, it emits more heat to HTF.

Figure 13 illustrates the numerical and experimental heat transfer obtained from HTF through PCM discharging at flow rates of 2 and 4 L/min. During the initial stage, heat transfer is mostly dominated by convective heat transfer, resulting in a high heat transfer rate across all geometric shapes. Over time, the rate of heat transfer decreases because of the existence of PCM layer near the inner tube wall. Moreover, the results show heat gained from HTF during paraffin wax discharging increased with decrease the mass flow rate of HTF for all geometrical shapes tested during discharging operation. The maximum achievable heat transfer obtained was 1117.8 kJ, occurring at a temperature of 310 degrees Celsius. This was seen in the shell/circular inner tube configuration, with a liquid percentage of 0.25 and a flow rate of 2 L/min.

During the discharge process, the objective is to transfer all the absorbed energy to HTF in accordance with the principle of energy conservation, which states that the energy gained must be equal to the energy lost. However, the occurrence of this phenomenon is prevented due to the absorption of energy by the aluminium shell and the copper inner tube in the exchanger. Figure 14 displays the cumulative energy exchanged with PCM (experimental and numerical) throughout the discharging operation at flow rates of 2 and 4 L/min for all geometrical form tests. In all geometric shapes, the rate of cumulative energy transfer from the paraffin wax to the HTF is high at the start of the process because of convection heat transfer, which is the dominant form of heat transfer during this interval. After some time, the heat transfer rate slows down due to the presence of a PCM layer near the inner tube wall. Additionally, the low thermal conductivity of PCM all this leads to conduction heat transfer becoming the dominant process. Furthermore, the results display the net cumulative energy gain from paraffin wax to HTF through the PCM discharging operation increased with decrease the mass flow rate of HTF. At 310 minutes, the

shell/circular inner tube's maximum theoretical cumulative energy was 1045.2 kilojoules, with a liquid fraction of 0.25 and a flow rate of 2 liters per minute.

Figure 15 displays the experimental and numerical thermal efficiency during the discharging operation at flow rates of 2 and 4 L/min for all geometrical form tests. The results for all investigated geometric shapes exhibit a rapid initial rise in thermal efficiency. This phenomenon is caused by the transmission of heat through convection, which is dominant throughout much of this period. Over time, the rate of heat transmission reduces because of the low thermal conductivity of PCM and the proximity of the PCM layer to the inner tube wall. Consequently, this resulted in the regulation of the heat transfer mechanism by conduction. Also, the results demonstrated that the theoretical thermal efficiency exhibited an upward trend when the mass flow rate of HTF decreased. The shell/circular tube system achieved a maximum theoretical thermal efficiency of 67.7% at a liquid percentage of 0.25 and a flow rate of 2 L/min, after 310 minutes.

Table 4. presents the actual and theoretical heat transfer parameters of the LHSS unit during the discharging operation at different water volumetric flow rates (2 and 4 L/min) for all examined geometrical forms.

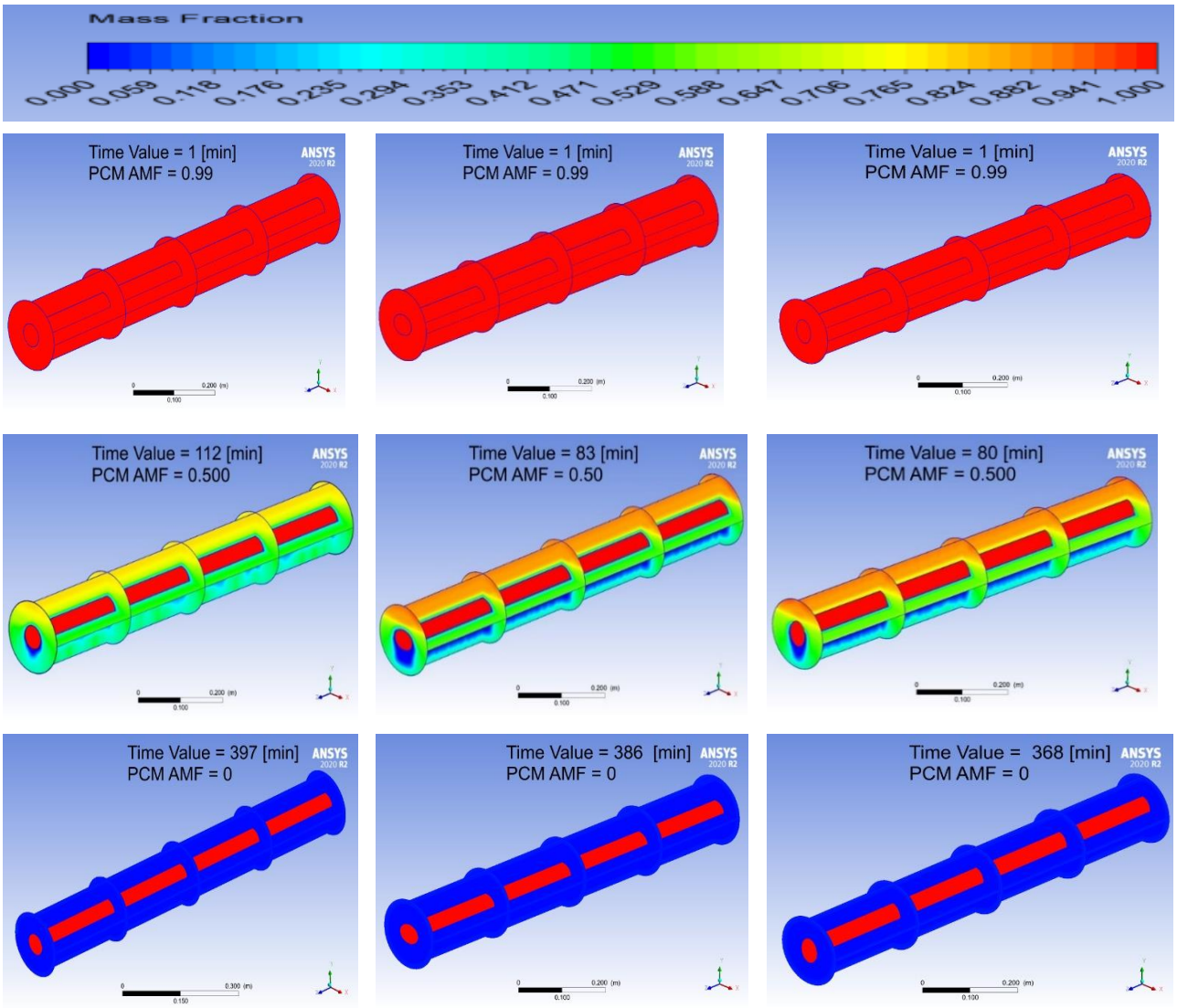

Shell/ circular tube | Shell/elliptical inner tube with minor axis bending. | Shell/elliptical inner tube with major axis bending.

Figure. 7. Mass fraction contour for three different geometric forms tested at a flow rate of 2 L/min

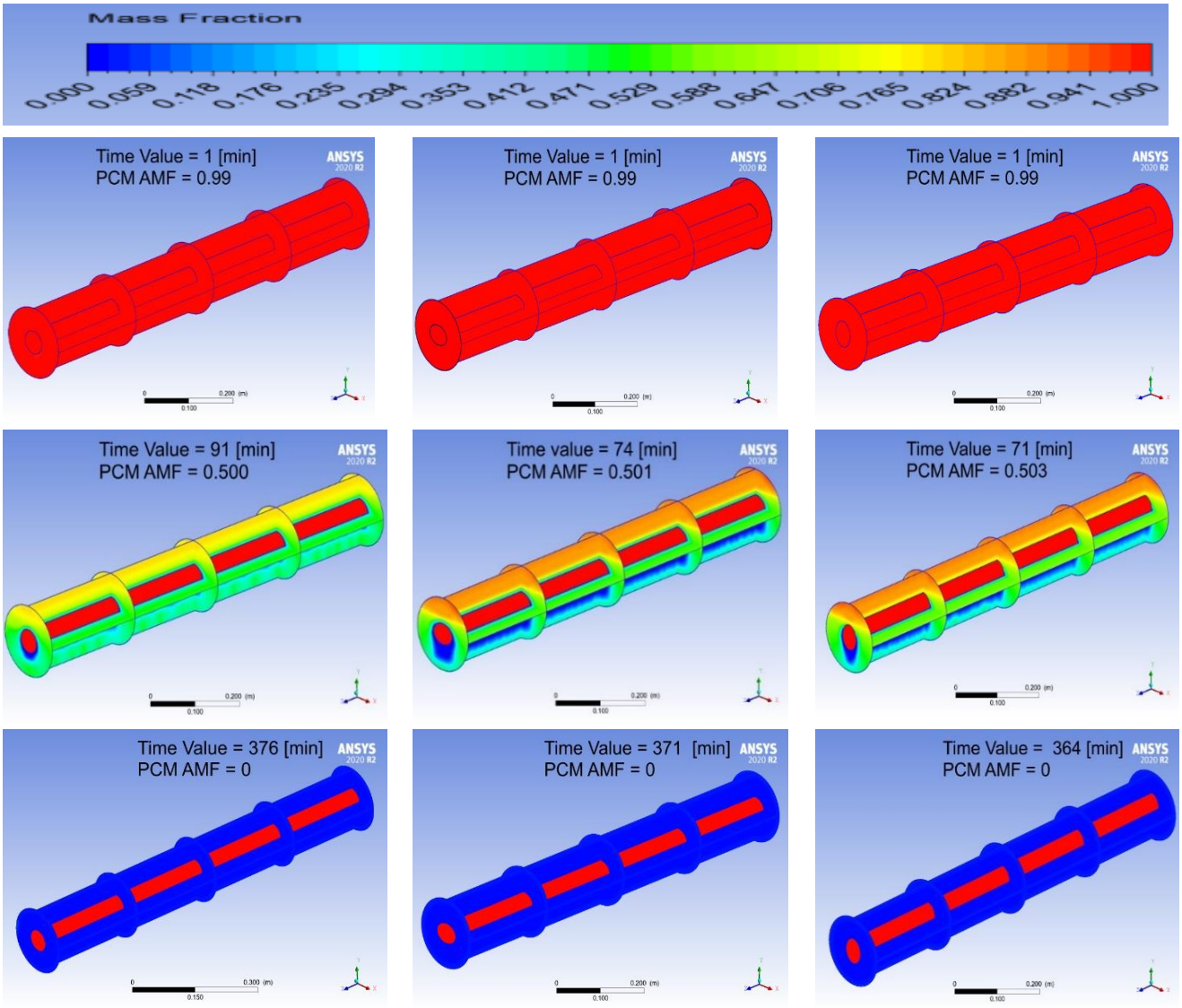

Shell/ circular tube | Shell/elliptical inner tube with minor axis bending. | Shell/elliptical inner tube with major axis bending.

Figure. 8. Mass fraction contour for three different geometric forms tested at a flow rate of 4 L/min.

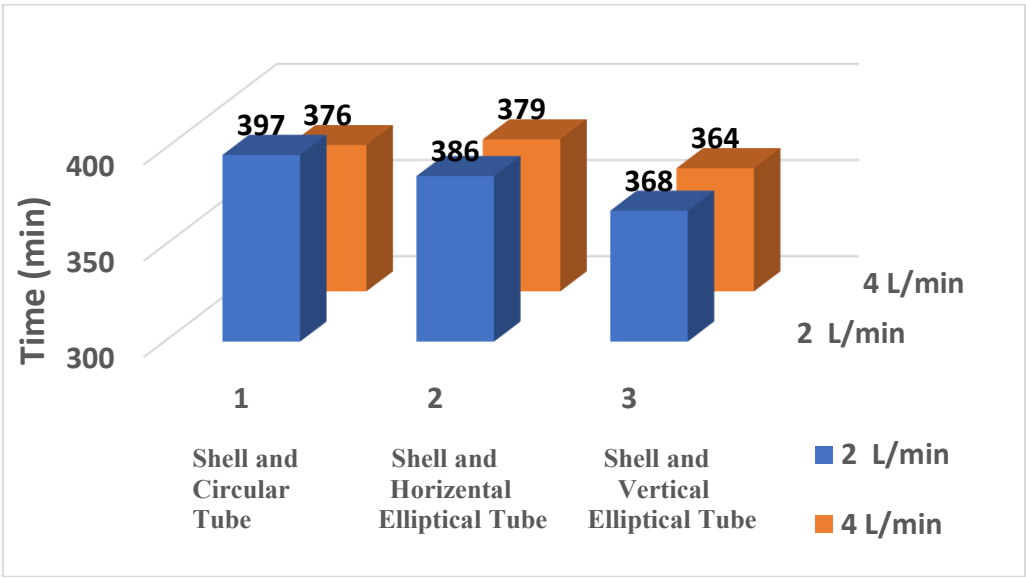

Figure. 9. Discharging time of PCM at HTF of (2 and 4 l/min).

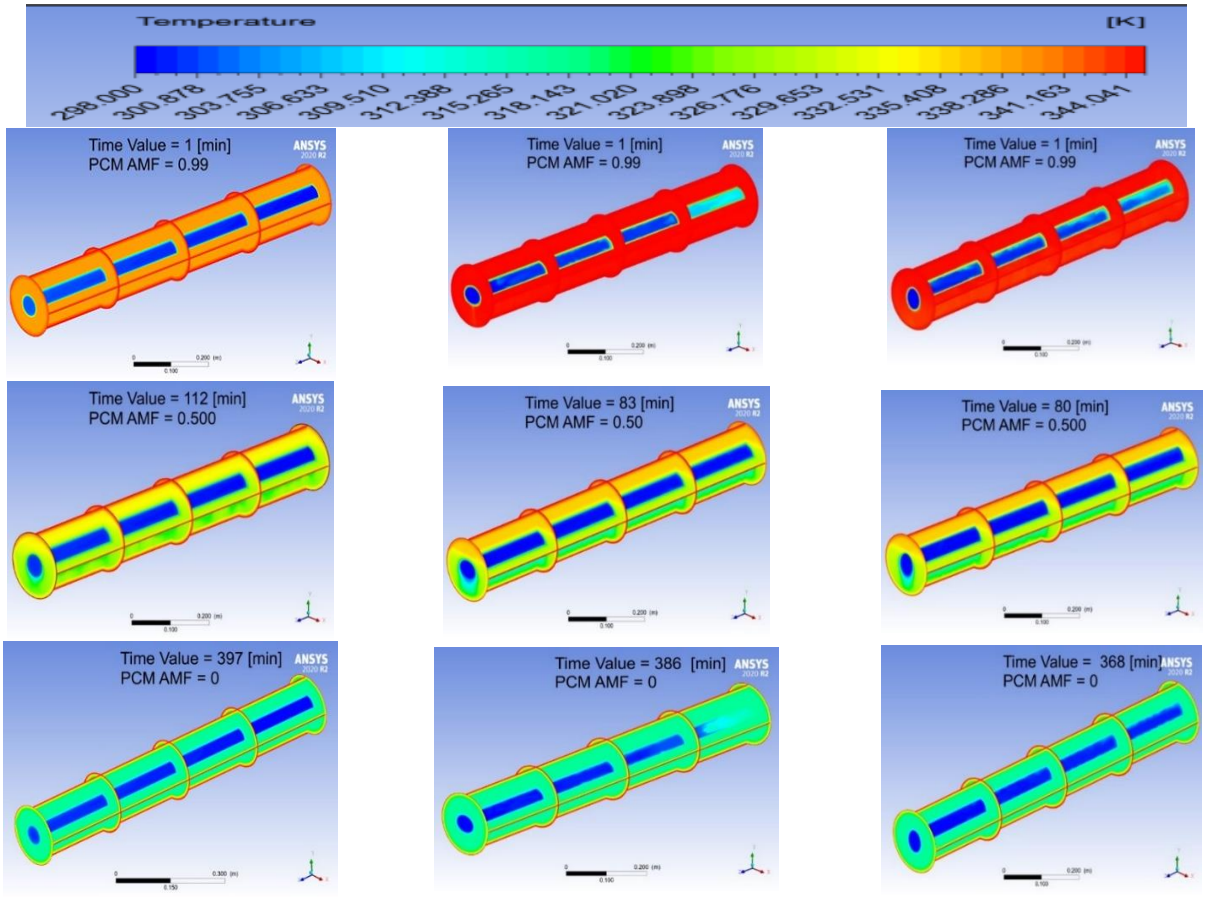

Shell/ circular tube

Shell/elliptical inner tube with minor axis bending.

Shell/elliptical inner tube with minor axis bending.

Figure. 10-A: Temperature contour for three different geometric shapes tested at a flow rate of 2 L/min.

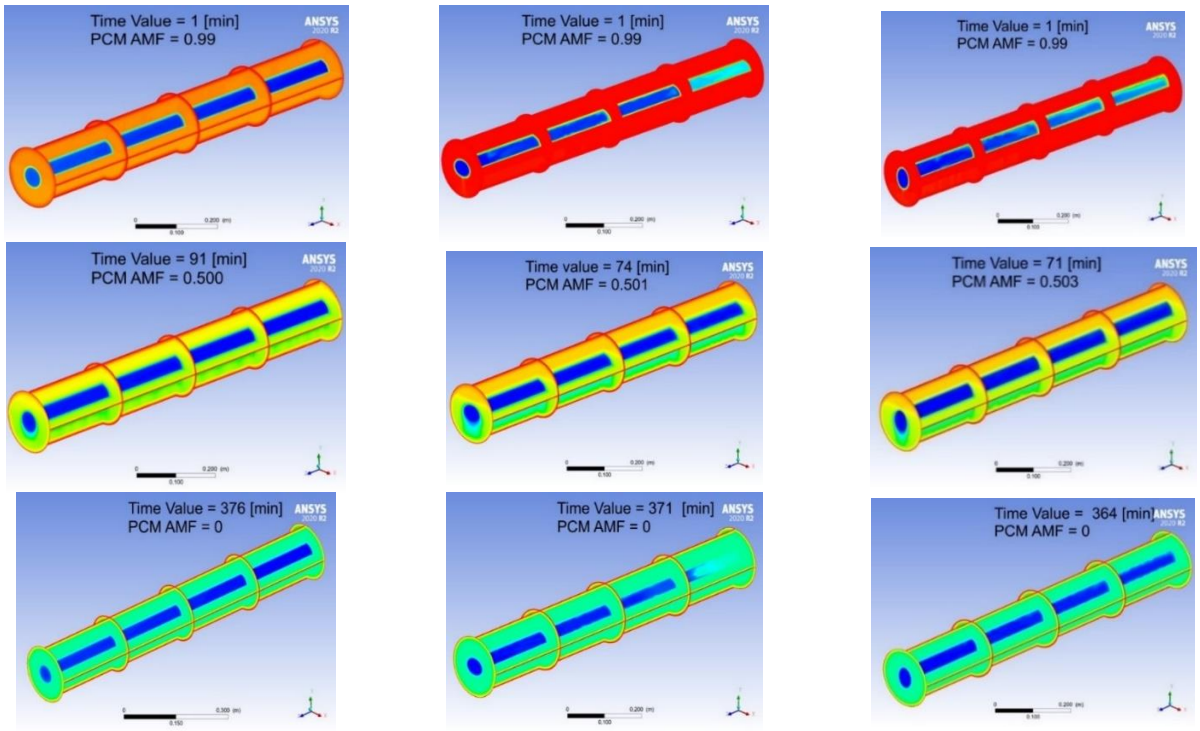

Shell/ circular tube

Shell/elliptical inner tube with minor axis bending.

Shell/elliptical inner tube with minor axis bending.

Figure. 10-B: Temperature contour for three different geometric shapes tested at a flow rate of 4 L/min.

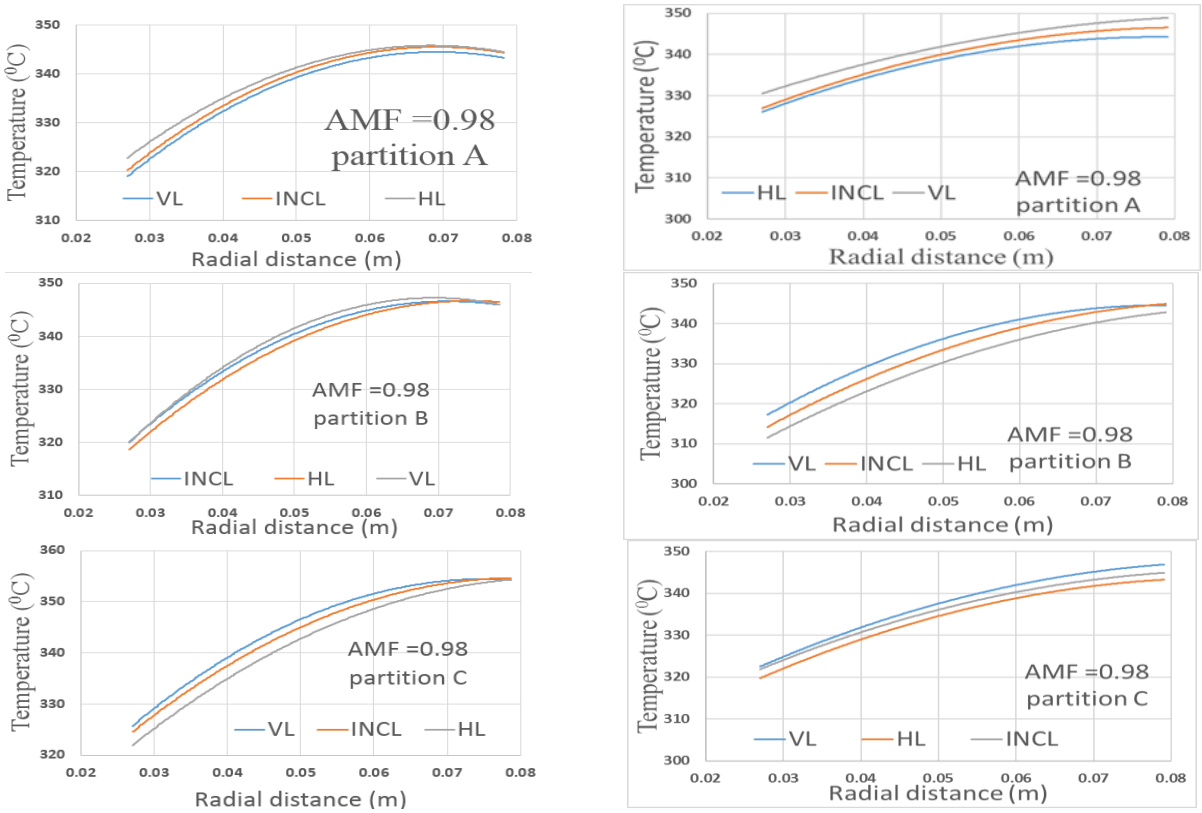

∀ = 2 L/min **∀ = 4 L/min**

Figure. 11-A: Radial temperature distribution at three partitions of LHSS unit with circular inner tube at (2 and 4 l/min) of HTF for average mass fraction 0.98.

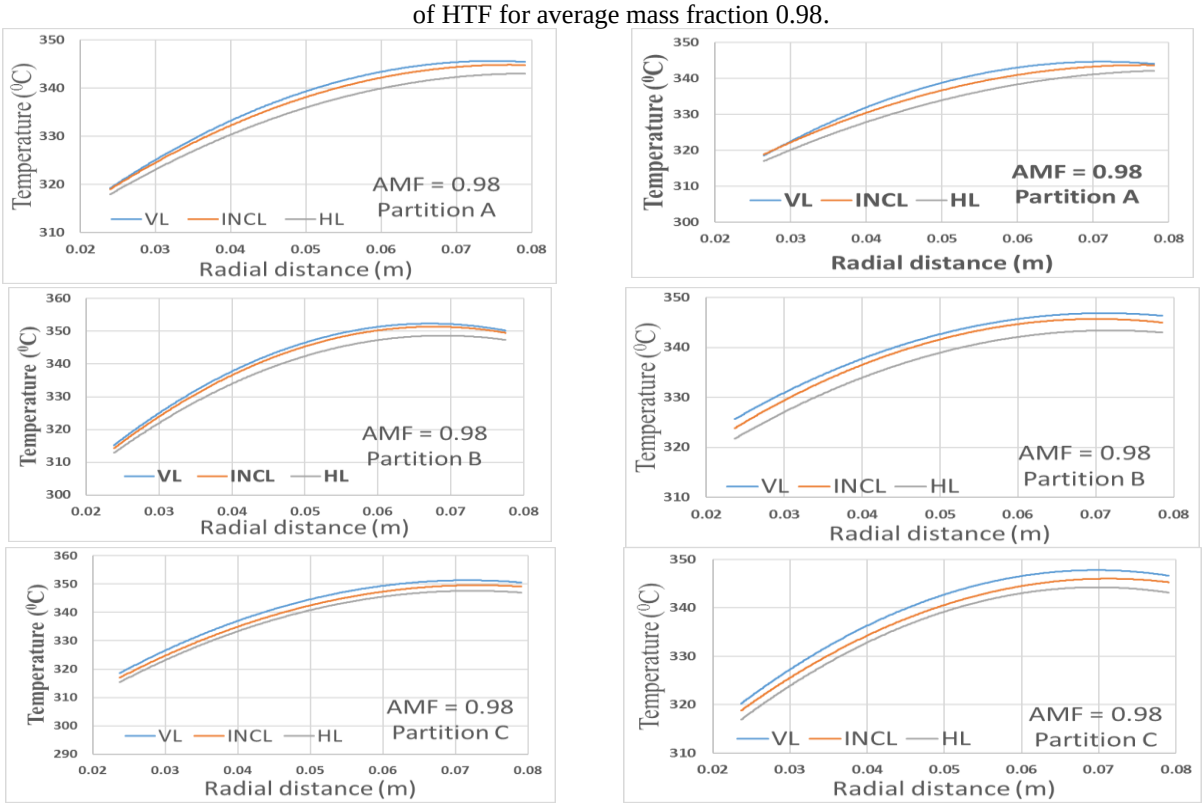

∀ = 2 L/min **∀ = 4 L/min**

Figure. 11-B: Radial temperature distribution at three partitions of LHSS unit with elliptical inner tube with major axis bending discharging process of PCM and four values of AMF, at (2 and 4 l/min) of HTF for average mass fraction 0.98.

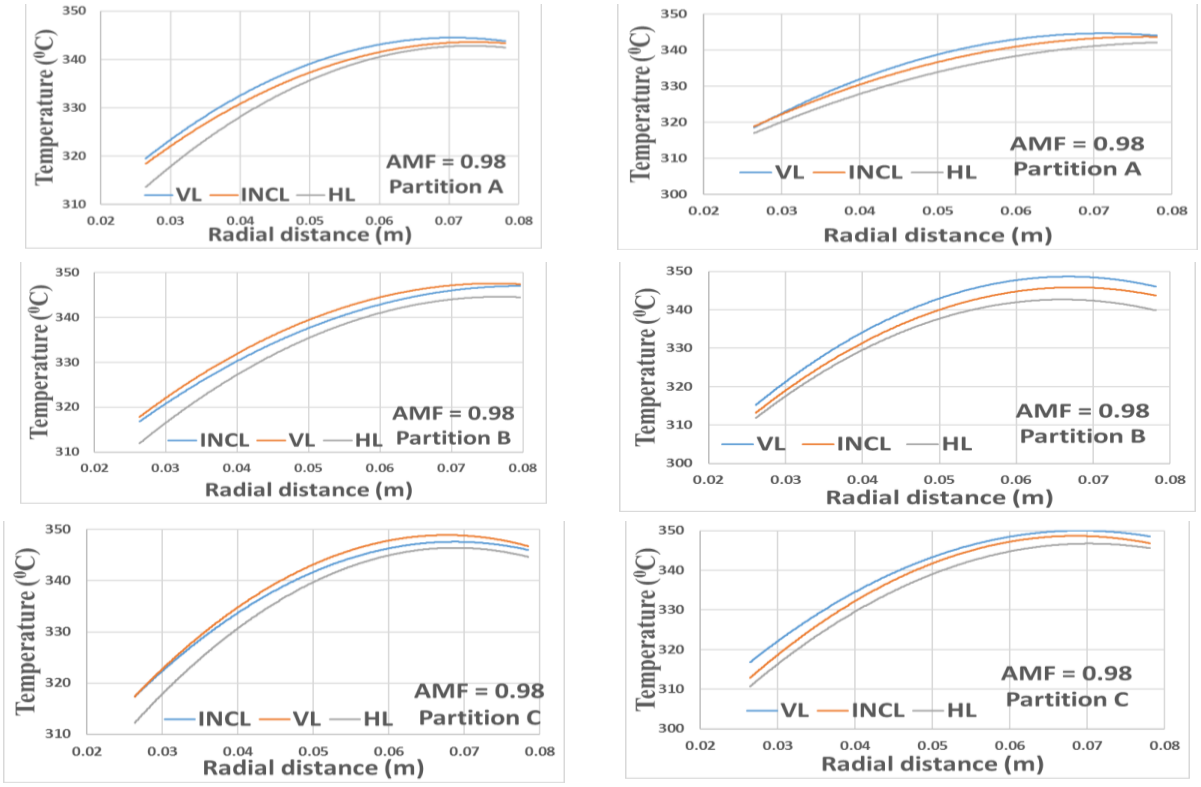

∀ = 2 L/min **∀ = 4 L/min**

Figure. 11-C: Radial temperature distribution at three partitions of LHSS unit with elliptical inner tube with minor axis bending discharging process of PCM and four values of AMF, at (2 and 4 l/min) of HTF for average mass fraction 0.98.

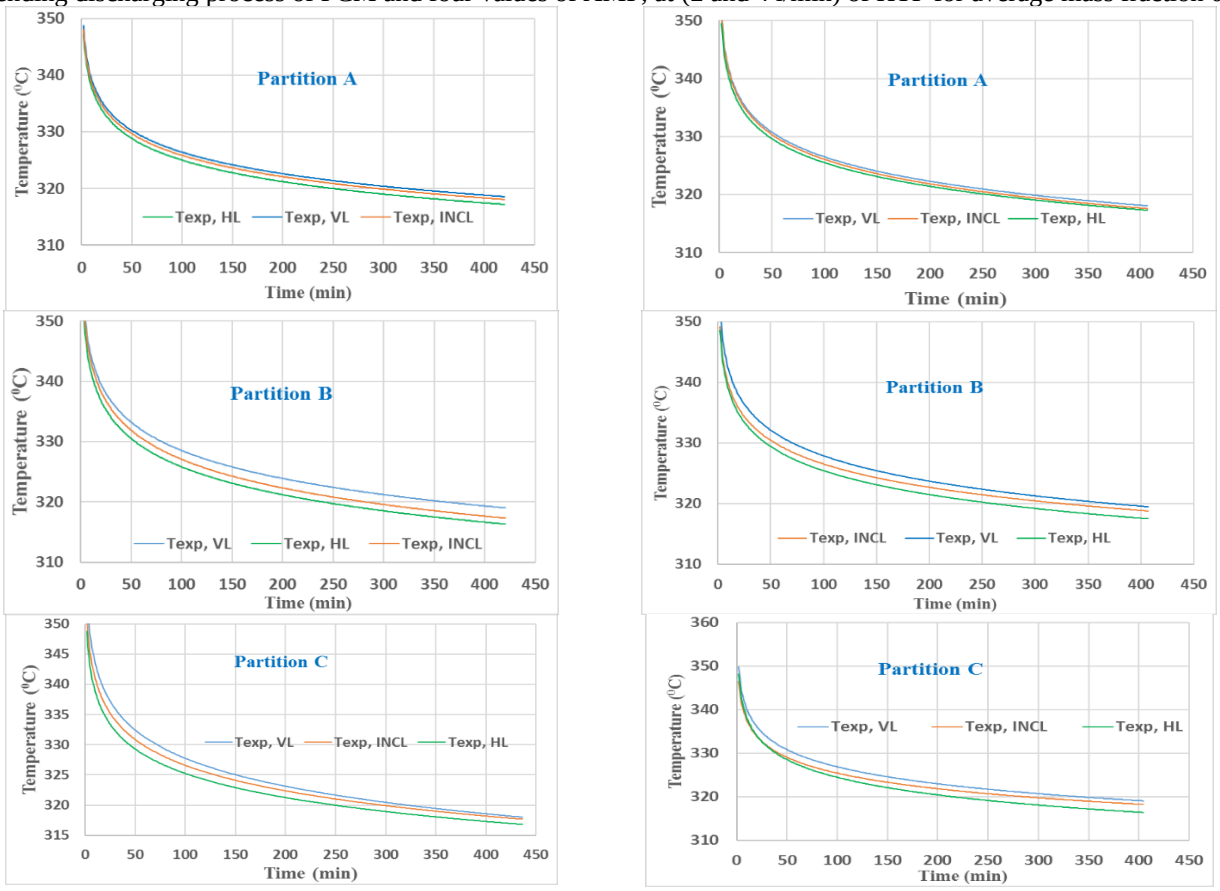

∀= 2 L/min **∀= 4 L/min**

Figure. 12-A: Experimental temperature variation with time at three partitions of LHSS unit (A, B, and C) with circular inner tube with minor axis bending solidification operation of PCM.

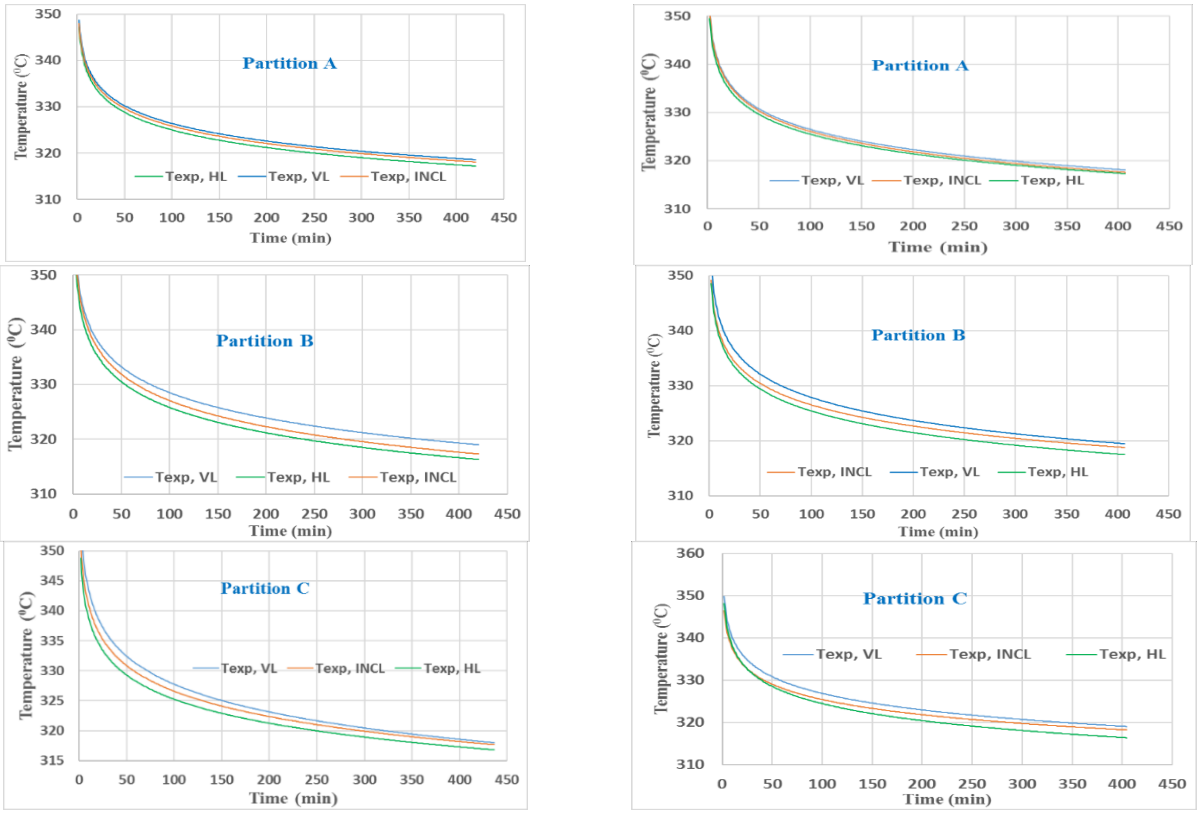

∀ = 2 L/min **∀ = 4 L/min**

Fig. 12-B: Experimental temperature variation with time at three partitions of LHSS unit (A, B, and C) with elliptical inner tube with minor axis bending solidification operation of PCM.

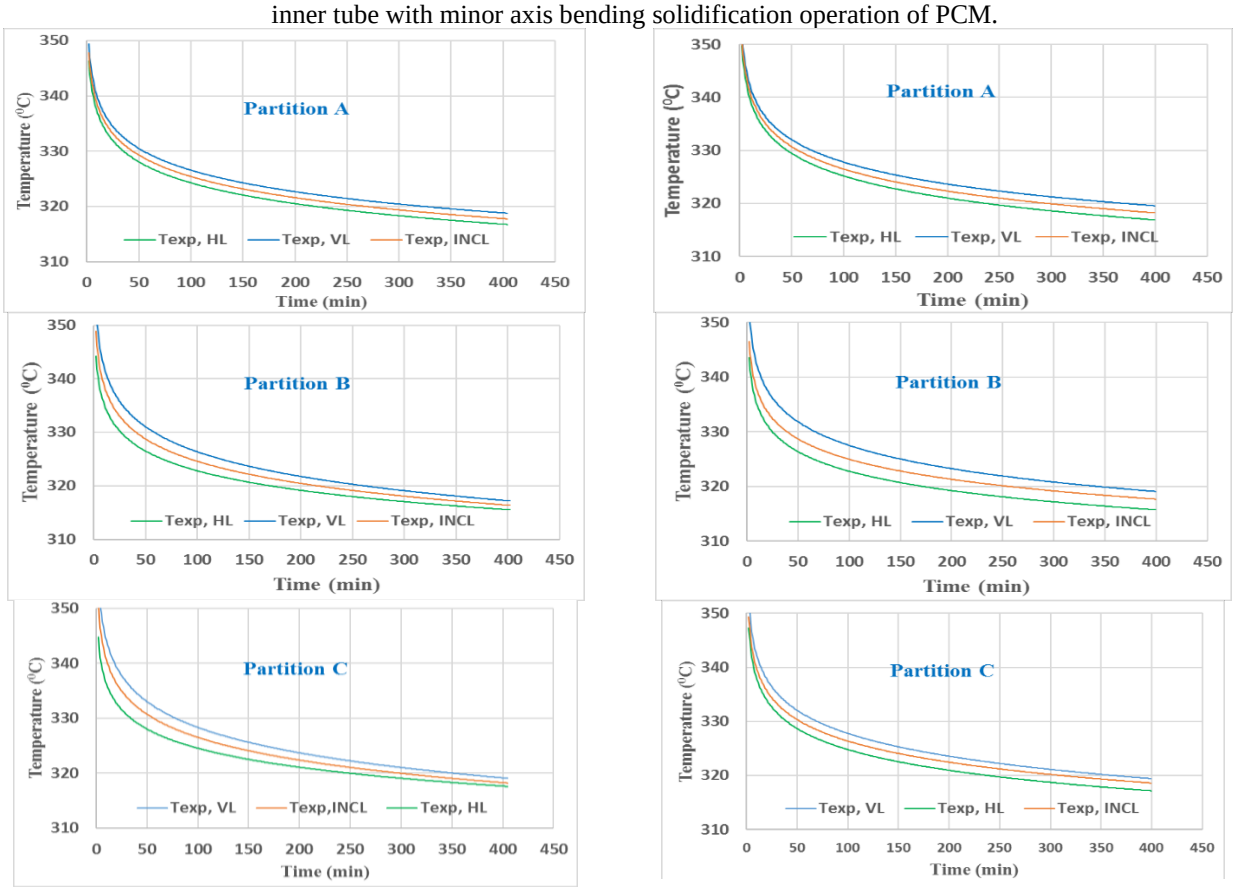

∀ = 2 L/min **∀ = 4 L/min**

Figure. 12-C: Experimental temperature variation with time at three partitions of LHSS unit (A, B, and C) with elliptical inner tube with major axis bending solidification operation of PCM.

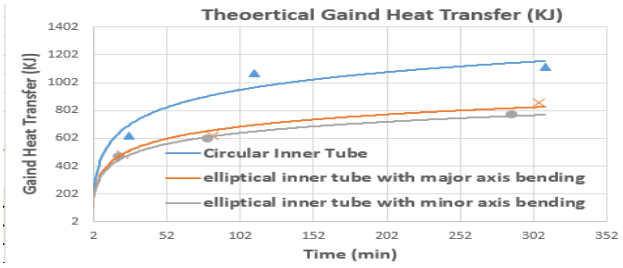

∀ = 2 L/min

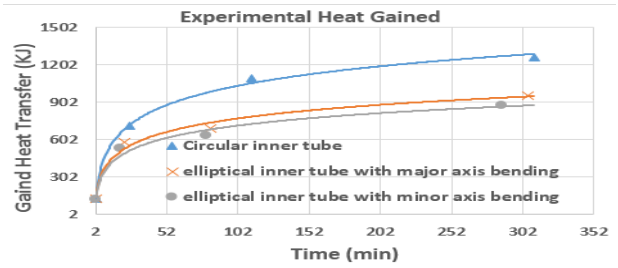

∀ = 2 L/min

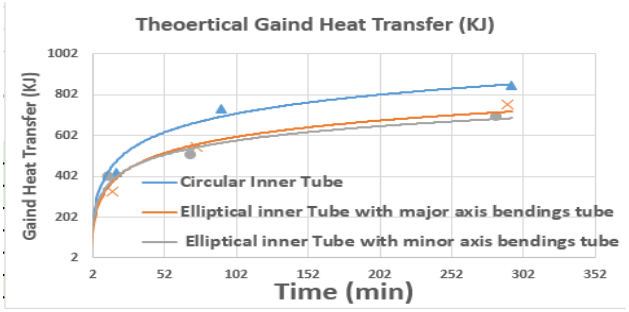

∀ = 4 L/min

(a) Theoretical heat transfer gained

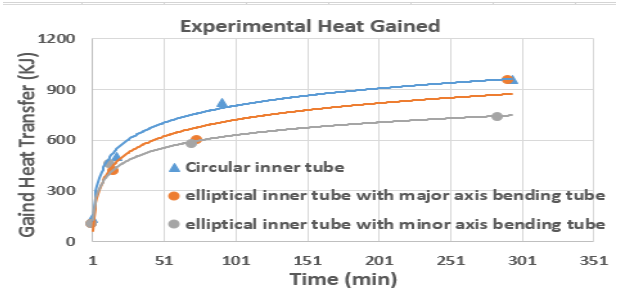

∀ = 4 L/min

(b) Experimental heat transfer gained

Figure. 13: (a) Theoretical heat transfer gained (b) Experimental heat transfer gained at 2 and 4 L/min.

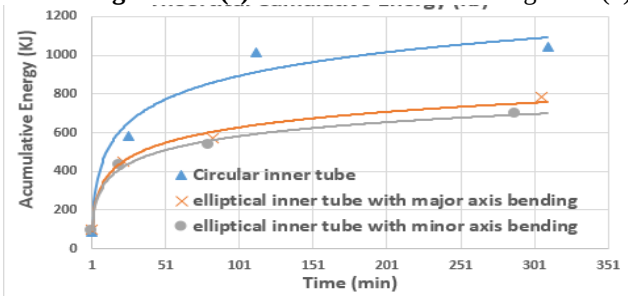

∀ = 2 L/min

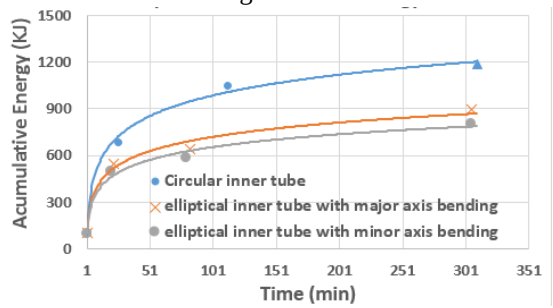

∀ = 2 L/min

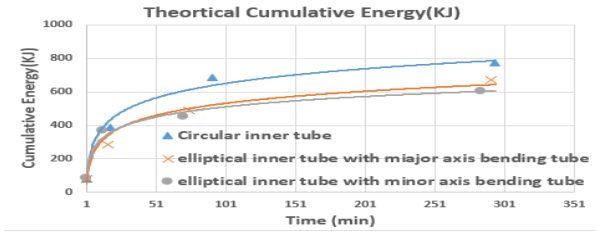

∀ = 4 L/min

(a) Theortical cumulative energy exchanged

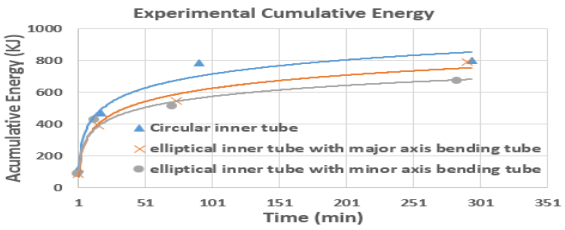

∀ = 4 L/min

(b) Experimental cumulative energy exchanged

Figure. 14: (a) Theoretical Cumulative Energy Exchanged (b) and Experimental Energy Exchanged at 2 and 4 L/min

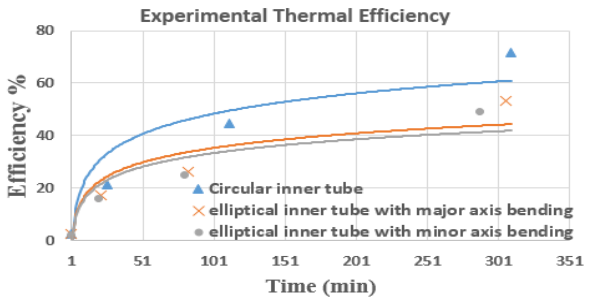

∀ = 2 L/min

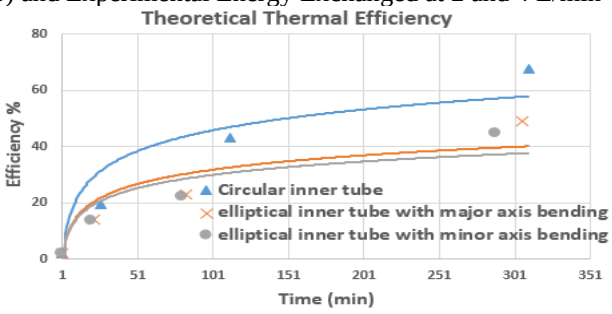

∀ = 2 L/min

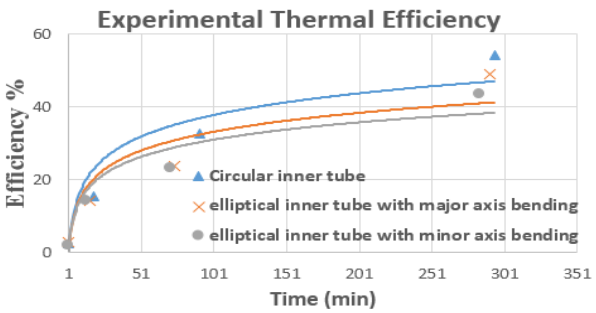

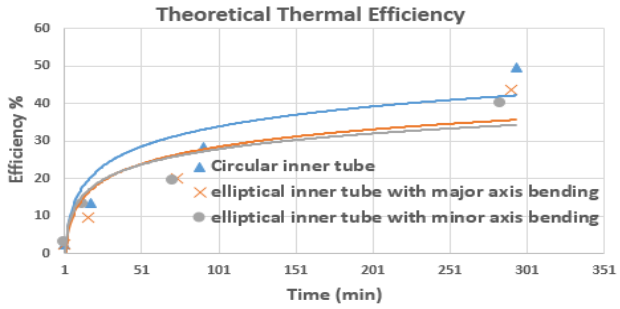

∀ = 4 L/min

(a) Experimental Thermal Efficiency (b) Theortical Thermal Efficiency

Figure. 15-A: (a) Theoretical Thermal Efficiency (b) Experimental Thermal Efficiency at 2 and 4 L/min

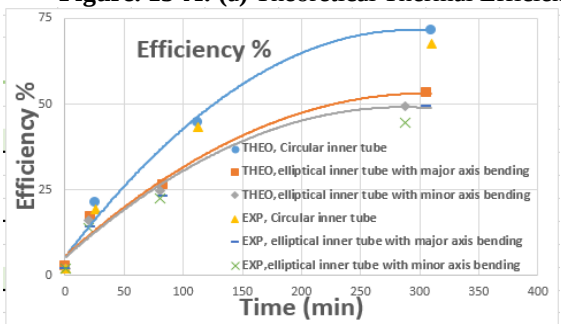

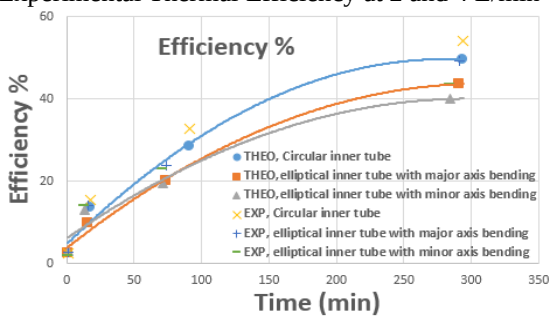

∀ = 2 L/min ∀ = 4 L/min

Figure. 15-B: Comparison between theoretical and experimental thermal efficiency at 2 and 4 L/min.

Table 4. Heat transfer characteristics and efficiency

HTF L/min	Geometrical shape	Time (min)	AMF	Gained Heat transfer (KJ)		Net Cumulative Energy (KJ)		Thermal Efficiency %		Efficiency Percentage Error
				Theo	EXP	Theo	EXP	Theo	EXP	
2	Shell and circular tube	1	0.98	104.3	125.9	87.3	103.7	1.81	2.31	0.216
		26	0.75	618.2	708.7	585.1	683.9	19.4	21.3	0.089
		112	0.50	1070.1	1092.3	1017.4	1050	43.19	44.7	0.034
		310	0.25	1117.8	1260.8	1045.2	1190.2	67.7	71.6	0.054
	Shell and elliptical inner tube with major axis bending tube	1	0.98	103.5	123.6	99.3	103.9	2.1	2.5	0.160
		22	0.75	483.3	576.3	449.6	544.4	14.02	17.01	0.176
		83	0.50	622.8	689.7	569.3	642.1	23.03	26.3	0.124
		306	0.25	859.1	955.1	785.1	893.6	49.2	53.2	0.075
	Shell and elliptical inner tube with minor axis bending tube	1	0.98	98.2	115.3	92.5	95.02	1.92	2.01	0.045
		20	0.75	464.1	530.1	431.3	498.4	13.6	15.9	0.142
		80	0.50	593.4	629.4	539.6	582.7	22.3	24.8	0.101
		288	0.25	770.5	872.7	696.4	801.3	44.6	48.1	0.093
4	Shell and circular tube	1	0.98	97.3	139.3	77.5	117.5	2.53	2.46	0.028
		18	0.75	423.2	503.2	387.3	469.7	13.4	15.3	0.124
		91	0.50	731.8	825.4	684.9	783.1	28.3	32.7	0.135
		294	0.25	849.4	958.6	772.6	800.39	49.6	54.2	0.085
	Shell and elliptical inner tube with major axis bending tube	1	0.98	82.5	102.1	77.3	85.3	2.5	2.73	0.084
		16	0.75	325.7	415.3	285.3	391.2	9.7	14.1	0.312
		74	0.50	546.8	597.6	492.7	547.5	20.1	23.7	0.152
		291	0.25	752.9	953.1	674.1	789.1	43.6	49.1	0.112
	Shell and elliptical inner tube with minor axis bending tube	1	0.98	88.3	102.4	83.4	85.3	2.98	2.01	0.483
		13	0.75	401.4	458.13	369.7	426.6	13.1	14.2	0.077
		71	0.50	504.5	576.3	453.1	512.8	19.4	23.1	0.160
		284	0.25	693.8	732.18	604.4	671.2	40.1	43.5	0.080

5. Conclusion

Based on the numerical simulation and experimental results, analysed how the mass flow rate and different geometric shapes of the inner tube affect the thermal performance of the LHSS unit during solidification. Several conclusions have been derived:

1. Natural convection dominates the heat transmission mechanism in all examined geometries during the solidification process, mostly due to the buoyancy force. Subsequently, the heat transfer is regulated by conduction, necessitating a longer duration to accomplish the solidification process.
2. For all tests, both the heat gained and net cumulative energy gain from paraffin wax to HTF decreased with increased the mass flow rate of HTF during the solidification process.
3. The circular inner tube has a slower response time for solidification because the center of the tube is far from the circular wall. In contrast, the center of the tube in the other shapes is closer to the wall.
4. The shell and circular tube exhibited the highest heat transfer process, resulting in the largest obtained and accumulated energy. This process achieved an efficiency of 66.37% for a duration of 240.5 minutes, specifically at a liquid percentage of 0.25. First, the inner tube undergoes bending along its major axis, followed by bending along its minor axis.
5. The maximum experimental and theoretical thermal efficiency of the paraffin wax discharging operation were in case the circular inner/shell tube with (71.6 % and 67.70 %) respectively at volumetric flow of the HTF (2 l/min) and 0.25 liquid fraction during 310 min. While, minimum experimental and theoretical efficiency of the PCM discharging operation were in case elliptical inner tube with minor axis bending/ shell with (43.5 % and 40.1 %) respectively, at flow of the HTF (4 l/min) and 0.25 liquid fraction during 284 min.

References

[1] K. Du, J. Calautit, Z. Wang, Y. Wu, and H. Liu, "A review of the applications of phase change materials in cooling, heating and power generation in different temperature ranges," Applied energy, vol. 220, pp. 242-273, 2018.

[2] Azain Sayekar, Akshay Mali, Nagesh Wadekar, Prashant Nalawade, Sateesha Patil (2019). A Review on PCM Heat Exchanger Using Paraffin Wax. Journal of Modern Thermodynamics in Mechanical System.

[3] G. Alva, Y. Lin, and G. Fang, "An overview of thermal energy storage systems," Energy, vol. 144, pp. 341-378, 2018.

[4] R. Senthil and M. Cheralathan, "Melting and Solidification of Paraffin Wax in a Concentric Tube PCM Storage for Solar Thermal Collector," International Journal of Chemical, vol. 14, no. 4, pp. 2634-2640, 2016.

[5] M. Rathod and J. Banerjee, "Experimental investigations on latent heat storage unit using paraffin wax as phase change material," Experimental heat transfer, vol. 27, no. 1, pp. 40-55, 2014.

[6] Y. Wang, L. Wang, N. Xie, X. Lin, and H. Chen, "Experimental study on the melting and solidification behavior of erythritol in a vertical shell-and-tube latent heat thermal storage unit," International Journal of Heat and Mass Transfer, vol. 99, pp. 770-781, 2016.

[7] J. M. Jalil and S. M. Salih, "Analysis of thermal and insulation performance of double glazed window doped with paraffin wax," Engineering and Technology Journal, vol. 38, no. 3, pp. 383-393, 2020.

[8] E. Tangsiriratana, W. Skolpap, R. J. Patterson, and K. Sriprapha, "Thermal properties and behavior of microencapsulated sugarcane wax phase change material," Heliyon, vol. 5, no. 8, 2019.

[9] A. H. Abed, "Thermal storage efficiency enhancement for solar air heater using a combined SHSm and PCM cylindrical capsules system: experimental investigation," Engineering and Technology Journal, vol. 34, no. 5, pp. 999-1011, 2016.

[10] H. Abbas, J. M. Jalil, and S. T. Ahmed, "Experimental investigation of the optimal location of PCM capsules in a hollow brick wall," Engineering and Technology Journal, vol. 39, no. 5, pp. 846-858, 2021.

[11] [A. K. Alshara and M. K. Kadhim, "Numerical investigation of energy storage in packed bed of cylindrical capsules of PCM," Engineering and Technology Journal, vol. 32, no. 2, pp. 494-510, 2014.

[12] M. S. Mahdi, H. B. Mahood, A. F. Hasan, A. A. Khadom, and A. N. Campbell, "Numerical study on the effect of the location of the phase change material in a concentric double pipe latent heat

thermal energy storage unit," Thermal Science and Engineering Progress, vol. 11, pp. 40-49, 2019.

[13] H. M. Sadeghi, M. Babayan, and A. Chamkha, "Investigation of using multi-layer PCMs in the tubular heat exchanger with periodic heat transfer boundary condition," International Journal of Heat and Mass Transfer, vol. 147, p. 118970, 2020.

[14] Z. Liu, X. Sun, and C. Ma, "Experimental study of the characteristics of solidification of stearic acid in an annulus and its thermal conductivity enhancement," Energy conversion and management, vol. 46, no. 6, pp. 971-984, 2005.

[15] A. Elmeriah, D. Nehari, and M. Aichouni, "Thermo-convective study of a shell and tube thermal energy storage unit," Periodica Polytechnica Mechanical Engineering, vol. 62, no. 2, pp. 101-109, 2018.

[16] M. Avci and M. Y. Yazici, "Experimental study of thermal energy storage characteristics of a paraffin in a horizontal tube-in-shell storage unit," Energy conversion and management, vol. 73, pp. 271-277, 2013.

[17] A. Agarwal and R. Sarviya, "An experimental investigation of shell and tube latent heat storage for solar dryer using paraffin wax as heat storage material," Engineering Science and Technology, an International Journal, vol. 19, no. 1, pp. 619-631, 2016.

[18] S. Seddegh, M. M. Joybari, X. Wang, and F. Haghighat, "Experimental and numerical characterization of natural convection in a vertical shell-and-tube latent thermal energy storage system," Sustainable cities and society, vol. 35, pp. 13-24, 2017.

[19] S. Jesumathy, M. Udayakumar, S. Suresh, and S. Jegadheeswaran, "An experimental study on heat transfer characteristics of paraffin wax in horizontal double pipe heat latent heat storage unit," Journal of the Taiwan Institute of Chemical Engineers, vol. 45, no. 4, pp. 1298-1306, 2014.

[20] M. Hosseini, M. Rahimi, and R. Bahrampoury, "Experimental and computational evolution of a shell and tube heat exchanger as a PCM thermal storage system," International Communications in Heat and Mass Transfer, vol. 50, pp. 128-136, 2014.

[21] J. S. Prasad, P. Muthukumar, R. Anandalakshmi, and H. Niyas, "Comparative study of phase change phenomenon in high temperature cascade latent heat energy storage system using conduction and conduction-convection models," Solar Energy, vol. 176, pp. 627-637, 2018.

[22] M. Esapour, M. Hosseini, A. Ranjbar, Y. Pahamli, and R. Bahrampoury, "Phase change in multi-tube heat exchangers," Renewable Energy, vol. 85, pp. 1017-1025, 2016.

[23] N. Kousha, M. Hosseini, M. Aligoodarz, R. Pakrouh, and R. Bahrampoury, "Effect of inclination angle on the performance of a shell and tube heat storage unit–An experimental study," Applied Thermal Engineering, vol. 112, pp. 1497-1509, 2017.

[24] A. M. S. Aljumaily, A. A. H. Al-Jubouri, and N. F. Al-Jubouri, "Improving the Thermal Storage System (LHTES): A theoretical and experimental study."

[25] M. Ajarostaghi, S. Soheil, M. Delavar, and A. Dolati, "Numerical investigation of melting process in phase change material (PCM) cylindrical storage considering different geometries," Heat Transf. Res, vol. 48, pp. 1515-1529, 2017.

[26] M. Y. Yazici, M. Avci, O. Aydin, and M. Akgun, "On the effect of eccentricity of a horizontal tube-in-shell storage unit on solidification of a PCM," Applied Thermal Engineering, vol. 64, no. 1-2, pp. 1-9, 2014.

[27] G. Shen, X. Wang, and A. Chan "Experimental investigation of heat transfer characteristics in a vertical multi-tube latent heat thermal energy storage system," Energy Procedia, vol. 160, pp. 332-339, 2019.

[28] M. Kibria, M. Anisur, M. Mahfuz, R. Saidur, and I. Metselaar, "Numerical and experimental investigation of heat transfer in a shell and tube thermal energy storage system," International Communications in Heat and Mass Transfer, vol. 53, pp. 71-78, 2014.

[29] A. D. Korawan, S. Soeparman, W. Wijayanti, and D. Widhiyanuriyawan, "3D numerical and experimental study on paraffin wax melting in thermal storage for the nozzle-and-shell, tube-and-shell, and reducer-and-shell models," Modelling and Simulation in Engineering, vol. 2017, no. 1, p. 9590214, 2017.

[30] S. Seddegh, X. Wang, and A. D. Henderson, "Numerical investigation of heat transfer mechanism in a vertical shell and tube latent heat energy storage system," Applied thermal engineering, vol. 87, pp. 698-706, 2015.

[31] N. Kousha, M. Rahimi, R. Pakrouh, and R. Bahrampoury, "Experimental investigation of phase change in a multitube heat exchanger," Journal of Energy Storage, vol. 23, pp. 292-304, 2019.

[32] D. S. Mehta, K. Solanki, M. K. Rathod, and J. Banerjee, "Influence of orientation on thermal performance of shell and tube latent heat storage unit," Applied Thermal Engineering, vol. 157, p. 113719, 2019.

[33] I. Al Siyabi, S. Khanna, T. Mallick, and S. Sundaram, "An experimental and numerical study on the effect of inclination angle of phase change materials thermal energy storage system," Journal of Energy Storage, vol. 23, pp. 57-68, 2019.

[34] M. Jourabian, A. A. R. Darzi, O. A. Akbari, and D. Toghraie, "The enthalpy-based lattice Boltzmann method (LBM) for simulation of NePCM melting in inclined elliptical annulus," Physica A: Statistical Mechanics and its Applications, vol. 548, p. 123887, 2020.

[35] M. Ajarostaghi, S. Soheil, M. Delavar, and A. Dolati, "Numerical investigation of melting process in phase change material (PCM) cylindrical storage

considering different geometries," Heat Transf. Res, vol. 48, pp. 1515-1529, 2017.

[36] W. Da Veiga and J. Meyer, "Semicircular heat exchanger used in a water heated condenser pump."

[37] R. A. Albaldawi, A. K. Shyaa, and B. M. Hammendy, "Experimental Study on the Effect of Insertion of Copper Lessing Rings in Phase Change Material (PCM) on the Performance of Thermal Energy Storage Unit," Al-Khwarizmi Engineering Journal, vol. 11, no. 4, pp. 60-72, 2015.

[38] M. Longeon, A. Soupart, J.-F. Fourmigué, A. Bruch, and P. Marty, "Experimental and numerical study of annular PCM storage in the presence of natural convection," Applied energy, vol. 112, pp. 175-184, 2013.

[39] M. Esapour, A. Hamzehnezhad, A. A. R. Darzi, and M. Jourabian, "Melting and solidification of PCM embedded in porous metal foam in horizontal multi-tube heat storage system," Energy conversion and management, vol. 171, pp. 398-410, 2018.

[40] M. Ghalambaz and J. Zhang, "Conjugate solid-liquid phase change heat transfer in heatsink filled with phase change material-metal foam," International Journal of Heat and Mass Transfer, vol. 146, p. 118832, 2020.

[41] W.-W. Wang, K. Zhang, L.-B. Wang, and Y.-L. He, "Numerical study of the heat charging and discharging characteristics of a shell-and-tube phase change heat storage unit," Applied Thermal Engineering, vol. 58, no. 1-2, pp. 542-553, 2013.

[42] L. Begum, M. Hasan, and G. H. Vatistas, "Energy storage in a complex heat storage unit using commercial grade phase change materials: Effect of convective heat transfer boundary conditions," Applied Thermal Engineering, vol. 131, pp. 621-641, 2018.

[43] M. Akgün, O. Aydın, and K. Kaygusuz, "Experimental study on melting/solidification characteristics of a paraffin as PCM," Energy conversion and management, vol. 48, no. 2, pp. 669-678, 2007.

[44] L. Jian-you, "Numerical and experimental investigation for heat transfer in triplex concentric tube with phase change material for thermal energy storage," Solar Energy, vol. 82, no. 11, pp. 977-985, 2008.

[45] M. Hosseini, A. Ranjbar, K. Sedighi, and M. Rahimi, "A combined experimental and computational study on the melting behavior of a medium temperature phase change storage material inside shell and tube heat exchanger," International Communications in Heat and Mass Transfer, vol. 39, no. 9, pp. 1416-1424, 2012.

[46] M. Hosseini, M. Rahimi, and R. Bahrampoury, "Experimental and computational evolution of a shell and tube heat exchanger as a PCM thermal storage system," International Communications in Heat and Mass Transfer, vol. 50, pp. 128-136, 2014.

[47] S. J. H. Al-Jabair and A. Al-Taee, "Experimental study of heat transfer coefficients of shell and helically coiled tube heat exchangers," Journal Engineering and Technology, vol. 31, no. 1, pp. 172-196, 2013.

[48] M. Kibria, M. Anisur, M. Mahfuz, R. Saidur, and I. Metselaar, "Numerical and experimental investigation of heat transfer in a shell and tube thermal energy storage system," International Communications in Heat and Mass Transfer, vol. 53, pp. 71-78, 2014.

[49] N. F. A. Hamza and S. Aljabair, "Evaluation of thermal performance factor by hybrid nanofluid and twisted tape inserts in heat exchanger," Heliyon, vol. 8, no. 12, 2022.

[50] J. P. Holman, "Experimental methods for engineers," 1966.

[51] S. Seddegh, X. Wang, and A. D. Henderson, "A comparative study of thermal behaviour of a horizontal and vertical shell-and-tube energy storage using phase change materials," Applied Thermal Engineering, vol. 93, pp. 348-358, 2016.

[52] Holman, J.P., Experimental Methods for Engineers, Edited by Marty Lange. 8th ed. United States: McGraw-Hill Series in Mechanical Engineering, 2011.